Evolution of first-year and second-year snow properties on sea ice in the Weddell Sea during spring-summer transition

Marcel Nicolaus,[1,2] Christian Haas,[1,3] and Sascha Willmes[4]

Received 2 October 2008; revised 27 March 2009; accepted 28 May 2009; published 11 September 2009.

[1] Observations of snow properties, superimposed ice, and atmospheric heat fluxes have been performed on first-year and second-year sea ice in the western Weddell Sea, Antarctica. Snow in this region is particular as it does usually survive summer ablation. Measurements were performed during Ice Station Polarstern (ISPOL), a 5-week drift station of the German icebreaker RV *Polarstern*. Net heat flux to the snowpack was 8 W m^{-2}, causing only 0.1 to 0.2 m of thinning of both snow cover types, thinner first-year and thicker second-year snow. Snow thinning was dominated by compaction and evaporation, whereas melt was of minor importance and occurred only internally at or close to the surface. Characteristic differences between snow on first-year and second-year ice were found in snow thickness, temperature, and stratigraphy. Snow on second-year ice was thicker, colder, denser, and more layered than on first-year ice. Metamorphism and ablation, and thus mass balance, were similar between both regimes, because they depend more on surface heat fluxes and less on underground properties. Ice freeboard was mostly negative, but flooding occurred mainly on first-year ice. Snow and ice interface temperature did not reach the melting point during the observation period. Nevertheless, formation of discontinuous superimposed ice was observed. Color tracer experiments suggest considerable meltwater percolation within the snow, despite below-melting temperatures of lower layers. Strong meridional gradients of snow and sea-ice properties were found in this region. They suggest similar gradients in atmospheric and oceanographic conditions and implicate their importance for melt processes and the location of the summer ice edge.

Citation: Nicolaus, M., C. Haas, and S. Willmes (2009), Evolution of first-year and second-year snow properties on sea ice in the Weddell Sea during spring-summer transition, *J. Geophys. Res.*, *114*, D17109, doi:10.1029/2008JD011227.

1. Introduction

[2] Snow on sea ice plays a key role within the climate and ecosystems of the polar oceans and enhances the role of sea ice for interactions between the ocean and the atmosphere. Snow positively contributes to sea-ice mass balance through the formation of snow ice [*Eicken et al.*, 1994; *Jeffries et al.*, 1997] and superimposed ice [*Haas et al.*, 2001; *Koerner*, 1970; *Nicolaus et al.*, 2003], although it simultaneously reduces thermodynamic ice growth by its low thermal conductivity [*Eicken et al.*, 1995; *Maykut and Untersteiner*, 1971; *Maykut*, 1986]. Snow ice forms during winter when a heavy snow load depresses the ice surface below the water level, causing negative freeboard and subsequent flooding, and subsequent refreezing of the resulting slush. Superimposed ice formation occurs during summer when the snow melts internally and percolating meltwater refreezes at the colder snow and ice interface.

[3] Even if the thermal and radiative energy transfer within the atmosphere-ice-ocean system is dominated by air temperature and radiation fluxes, snow properties and metamorphism affect these transfers significantly. The snow cover determines surface albedo, heat conduction, and optical properties [e.g., *Grenfell and Perovich*, 1984; *Perovich*, 1996]. Snow accumulation, redistribution, and compaction greatly modify the aerodynamic roughness of the sea-ice surface, and this strongly affects the momentum flux from the atmosphere to sea ice [*Vihma et al.*, 1996]. Spring-to-summer evolution of snow and ice properties in the western Weddell Sea is generally characterized by low atmospheric energy input, because turbulent fluxes are predominantly from snow to air and compensate most of the energy entry through short-wave radiation. Snow ablation is dominated by evaporation while melt is of minor importance [*Andreas and Ackley*, 1982; *Nicolaus et al.*, 2006].

[4] Since sea ice is snow covered during most times of the year, snow properties largely control its microwave signatures [*Barber et al.*, 1998; *Haas et al.*, 2001, 2008a; *Willmes et al.*, 2006]. Hence they play an important role for the analysis and interpretation of satellite data of the polar

[1] Alfred Wegener Institute for Polar and Marine Research, Bremerhaven, Germany.
[2] Norwegian Polar Institute, Tromsø, Norway.
[3] Earth and Atmospheric Sciences, University of Alberta, Edmonton, Alberta, Canada.
[4] Environmental Meteorology, University of Trier, Trier, Germany.

Copyright 2009 by the American Geophysical Union.
0148-0227/09/2008JD011227

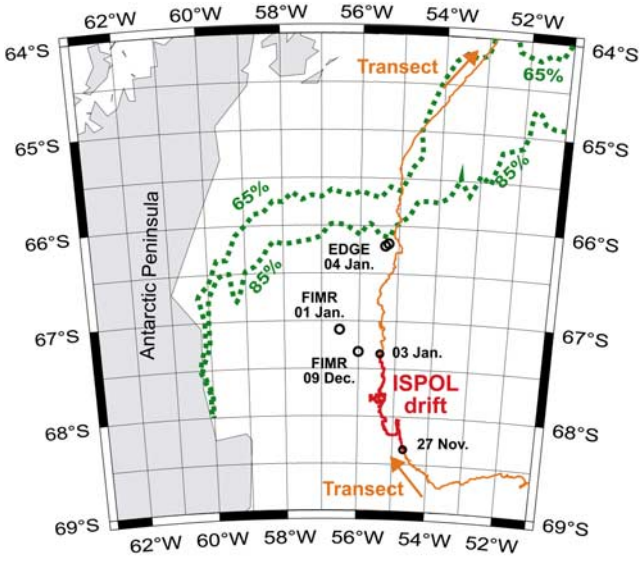

Figure 1. Map of the western Weddell Sea including the Ice Station Polarstern (ISPOL) (RV *Polarstern*) cruise track (transect in orange and drift in red) from November 2004 to January 2005, sea-ice concentration on 4 January 2005 (dotted green lines), and locations of helicopter ice stations (black circles with date and name of the station). The first and the last day of the drift phase are marked (labeled black circles), and arrows indicate steaming/drift direction. Additional maps may be found in the work of *Hellmer et al.* [2008].

oceans. Seasonally varying snow properties and especially the onset of (snow) melt can be detected and used for large-scale climate studies [*Anderson and Drobot*, 2001; *Bareiss and Görgen*, 2008; *Winebrenner et al.*, 1998]. Knowledge of snow properties is required as input for models of snow microwave properties as demonstrated by *Tonboe et al.* [2006].

[5] Most studies of snow on Antarctic sea ice have been performed before melt season [*Allison et al.*, 1993; *Eicken et al.*, 1994; *Massom et al.*, 1998, 2001; *Sturm et al.*, 1998]. Their results were considerably different from snow properties observed during summer [*Haas et al.*, 2001; *Massom et al.*, 2001; *Morris and Jeffries*, 2001]. Snow accumulation, metamorphism, and ablation lead to significant, irreversible changes of optical, thermal, and microwave properties of snow during the spring and summer transition, when the surface energy balance becomes positive and albedo feedback mechanisms may be triggered. Few observations of these changes have been performed so far, since they ideally require continuous observations at one location. In addition, measurements during spring and summer are particularly difficult, because snow and ice are at their melting temperatures, and measurements can be hampered by absorption of solar radiation. Enhanced melt may occur around sensors.

[6] One of the most prominent features of perennial Antarctic sea ice in summer is the occurrence of superimposed ice [*Haas et al.*, 2001; *Kawamura et al.*, 1997]. It has been postulated that superimposed ice can only form from isothermal snow close to its melting temperature, which would also allow percolation of meltwater to the snow-ice interface [*Haas et al.*, 2001; *Nicolaus et al.*, 2003]. However, the exact formation process and the precondition of isothermal snow have not been proven so far.

[7] Similar drift station studies have been performed on Arctic sea ice, too. SHEBA [*Perovich et al.*, 1999], the Russian North Pole drift stations [*Frolov et al.*, 2005], and Tara [*Gascard et al.*, 2008] are probably the most prominent ones. But sea-ice properties and snow covers differ significantly in both polar regions, especially during summer. On Arctic sea ice, snow melts completely during summer, forming characteristic melt ponds. In contrast, on Antarctic sea ice, snow often survives summer because of higher accumulation and lower ablation rates [*Jeffries et al.*, 1994; *Massom et al.*, 2001; *Nicolaus et al.*, 2006; *Warren et al.*, 1999]. In addition, oceanic boundary conditions are significantly different. The Arctic Ocean is characterized by fresh water overlying a strong pycnocline, while the Southern Ocean is typically characterized by a large ocean heat flux.

[8] Here we present changes of snow properties, superimposed ice formation, and meltwater percolation, performed during the spring and summer transition on first-year and second-year sea ice in the western Weddell Sea. We discuss them in relation to variations of the surface energy balance and characterize significant similarities and differences. Simultaneous changes of sea-ice properties have been presented by *Haas et al.* [2008a], *Hellmer et al.* [2008], and *Tison et al.* [2008]. This study describes observations on a floe scale, neglecting effects of ocean heat flux due to absorption of radiation in open water and leads, which would be necessary for a larger, aggregate scale study [*Perovich*, 2005]. Anyhow, ocean heat fluxes are comparably low in the western Weddell Sea, also compared to the East Antarctic [e.g., *McPhee*, 2008; *Ohshima et al.*, 1998].

[9] The observational program was part of the interdisciplinary Ice Station Polarstern (ISPOL) project conducted in the western Weddell Sea in austral spring and summer of 2004/2005. The main goal of the cruise was to study physical-biological sea-ice processes at the onset of summer melt as a function of atmospheric and oceanic boundary conditions during a 35-day-long drift station from 28 November 2004 (54.84°W; 68.21°S) to 2 January 2005 (55.41°W; 67.36°S; see map in Figure 1). During this time the German icebreaker RV *Polarstern* was anchored to an originally 10 × 10-km large ice floe, the ISPOL floe, which was selected to be as characteristic for the region as possible [*Hellmer et al.*, 2008]. The floe was composed of patches of thick and thin first-year ice (FYI) embedded in a matrix of second-year ice (SYI). Modal total (snow plus sea ice) thickness ranged from 1.2 to 1.3 m over 2.1 m to 2.4–2.9 m for FYI and SYI, respectively [*Haas et al.*, 2008a]. Most of the SYI originated from the central and southern Weddell Sea. The thicker FYI was advected from the coastal polynya at the Ronne Ice Shelf, and the thin FYI was locally formed [*Haas et al.*, 2008a].

[10] In addition to the measurements on the ISPOL floe, three floes approximately 100 km north of the ISPOL floe were visited by helicopter to investigate meridional gradients of snow properties and superimposed ice formation.

2. Methods

[11] Repeated measurements of physical snow properties were performed on several level-ice sites of the ISPOL floe,

Table 1. Characteristic Snow and Sea-Ice Properties of the ISPOL Floe[a]

	Snow[c]							Sea Ice[d]		
Site[b]	Type	z_0 (cm), Date	z_{end} (cm), Date	dz (cm/d)	ρ_0 (kg/m^3), m_0 (kg)	ρ_{end} (kg/m^3), m_{end} (kg)	dm (kg)	Type	zi (cm)	fb
FY1 (S6)	FYS	31.7 ± 3.9, 29 November	13.5 ± 8.0, 30 December	−0.51	250, 79.3	385, 52.0	−27.3	FYI	95	neg
FY2 (S9)	FYS	14.0 ± 4.53, 11 December	7.2 ± 4.3, 2 January	−0.33	n.d., n.d.	n.d., n.d.	n.d.	FYI	116	pos
SY1 (S8)	SYS	81.0 ± 11.0, 3 December	64.0 ± 11.0, 28 December	−0.64	337, 273.0	376, 240.6	−32.4	SYI	248	neg
SY2 (S5)	SYS	94.6 ± 6.2, 29 November	84.2 ± 10.4, 31 December	−0.49	n.d., n.d.	n.d., n.d.	n.d.	SYI	190	neg

[a]For exact location of measurement sites on the floe, see map in the work of *Hellmer et al.* [2008]. Abbreviations are as follows: FYS, first-year snow; SYS, second-year snow; FYI, first-year ice; SYI, second-year ice; subscripts "0" and "end" denote values at the beginning and end of the observation period, respectively; z, snow thickness; ρ, snow density; m, snow mass; zi, sea-ice thickness; fb, freeboard; neg, negative; pos, positive; n.d., not determined.

[b]Additional site names (S6, S9, ...) denote original site names, as used during the field experiment, and should ease links to other studies during Ice Station Polarstern (ISPOL).

[c]Snow thinning rate (dz) was derived from linear regression, and snow mass balance (dm) was derived from equation (1). Time series of snow thicknesses are shown in Figure 3, and those of snow densities are shown in Figure 9.

[d]Sea-ice characteristics are from *Haas et al.* [2008a].

separated from one another by ridges and rubble fields. The measurements were performed on two sites with first-year snow cover (FY1 and FY2) and on two sites with second-year snow cover (SY2 and SY1). These sites were chosen after inspection of the entire floe by helicopter with additional measurements of snow and sea-ice thickness, because all selected sites needed to be representative and well accessible during the observation period. Table 1 summarizes characteristic snow and sea-ice properties of the monitoring sites, including their original nomenclature, which is consistent with other studies during ISPOL [*Hellmer et al.*, 2008]. FY1 and SY1 were visited daily. SY2 and FY2 were studied only a few times during the observation period because of difficult access after the floe had fractured into smaller floes twice, on 2 and 24 December because of strong winds and changing wind directions. These breakup events also required relocation of parts of the equipment and field stations to other sites with the same snow types [*Hellmer et al.*, 2008].

[12] At each site, snow thickness was measured along a 50-m profile with a spacing of 1.0 m on level ice with the aid of a wooden ruler stick. Technical accuracy (marks on the ruler stick) of these measurements is 0.01 m, but taking into account the centimeter-to-decimeter small-scale variability of snow thickness, accuracy is only better than 0.02 m. Mean thickness and standard deviation are expected to be representative for the respective sites. Measurement frequency was adapted to changes in weather conditions and the occurrence of breakup events, in order to efficiently document all significant changes. Snow thickness measurements on FY1 were slightly biased by repeated crack formation across the profile and the subsequent movement of the profile to a nearby location on the same site. Mean values, as presented here, should not be affected, since the sites and profiles were selected to be representative.

[13] Vertical profiles of snow temperature, wetness, and density were measured in snow pits with a vertical resolution of 0.03 to 0.20 m, depending on the total snow thickness and stratigraphy, i.e., on the presence of individual snow layers. In order to investigate amplitude and phase of the diurnal snow temperature cycle, three hourly measurements were performed throughout daytime during the first 9 days of the study (until 7 December). Afterward, measurements were performed at least once per day during the time of the snow temperature maximum occurring around 1700 UTC (1300 local time (LT)) to investigate seasonal changes and detect snow metamorphism and superimposed ice formation. Snow stratigraphy was visually classified according to *Colbeck et al.* [1990] in the snow pits of FY1 and SY1 on some observation days.

[14] In each snow pit, vertical profiles of snow temperature were determined with a handheld Pt-1000 thermometer, protected from direct solar radiation. We consider manual measurements as the only means to obtain accurate temperature measurements in spring and summer, because fixed thermistor strings cause melting by radiation absorption and therefore lead to biased results. Snow density was determined from volumetric (volume: 0.5 L; diameter, 5 cm) measurements in continuous profiles to ease vertical averaging. Snow salinity was measured on all 52 volumetric snow density samples. The presence of ice layers frequently hampered volumetric measurements. In addition, snow wetness and density were measured with a dielectric resonator probe (TOIKKA Snow Fork, Espoo, Finland) [*Sihvola and Tiuri*, 1986]. Since the snow wetness measurements are only valid for unsaturated snow, all wetness readings above 15%$_{vol}$ were rejected from further analyses [*Colbeck et al.*, 1990]. Similarly, single readings of snow densities below 100 (except for new snow) and above 800 kg m^{-3} were filtered and neglected. Saltwater saturated layers (slush) could not be measured for methodical limitations. Single density measurements along vertical profiles often show large differences (>100 kg m^{-3}) between both methods. These differences cannot be discussed here, since the total amount of measurements is too small for a reliable comparison of both methods.

[15] Snow mass loss dm (per m^2) was calculated in snow-water equivalent as

$$dm = \rho_0 \times z_{s0} - \rho_n \times z_{sn} \quad (1)$$

from mean snow density ρ and mean snow thickness z_s, measured at the beginning (time 0) and end (time n) of the observations.

[16] Snow, sea ice, and superimposed ice were sampled by means of coring and subsequently sawn into vertical slices to study ice texture and stratigraphy at the snow-ice interface in detail. All samples were immediately brought to the ice laboratory on board RV *Polarstern* and stored at −15°C until analyzed as thin sections on the ship. Afterward,

salinity was measured on melted samples. Here only snow and sea-ice surface samples are discussed. Results for the underlying sea-ice column are summarized by *Haas et al.* [2008a].

[17] To study the percolation of meltwater and the permeability of snow as well as ice lenses and superimposed ice, dye tracer experiments were performed using Sulforhodamin-B (SR). SR has a low adsorbance (hydrophil) onto ice surfaces and is, compared to alternative fluorescents, much less sensitive to light decay. SR was already previously used by *Freitag and Eicken* [2003] and M. A. Granskog (personal communication, 2008) to study similar melt processes in snow on sea ice. SR experiments were performed close to the weather station on FY2 during the last week of ISPOL, after first prominent ice layers had developed in the snow and at the snow and ice interface. Four close locations (within 50 m) with snow thickness between 11 and 30 cm were studied. To initialize the experiment, 250 mL of a 100 mg L^{-1} solution of SR were sprayed homogenously over a 1 $\times$ 1-m snow surface (Figure 11a). The tracer solution was precooled to just above 0°C to prevent unnatural local melting as much as possible. Control measurements showed that initially only the uppermost 1 to 2 cm were contaminated with the color tracer. Afterward, several surface samples were drilled or sawn out every 3 h to 2 days to analyze the distribution of the tracer with a vertical resolution of 1 to 2 cm. Surface samples contained the entire snowpack down to a slush layer which was present on top of the sea ice at all four locations. Most of the snowpack was very heterogeneous and included several ice layers and a layer of superimposed ice at the bottom. Sea ice was not sampled for this tracer study.

[18] To study a possible meridional gradient of snow metamorphism and superimposed ice formation across the ISPOL region, one additional FYI floe, referred to as Finnish Institute of Marine Research (FIMR) floe, was visited twice during the observational period, on 9 December 2004 and 1 January 2005. This floe was located approximately 100 km north of the ISPOL floe (map in Figure 1) and was marked by a buoy reporting GPS coordinates, air pressure, and air temperature via satellite link [*Heil et al.*, 2008]. Furthermore, two floes close to the ice edge (66.2°S, 55.5°W, 120 km north of the end position of the ISPOL drift) were visited once on 4 January, 2 days after leaving the ISPOL floe (map in Figure 1). These floes will be referred to as EDGE floes.

[19] For continuous observations of atmospheric heat fluxes a meteorological station named AWI station was installed on FY1 from 29 November to 25 December 2004 and on FY2 after the breakup until 2 January 2005 (map in the work of *Hellmer et al.* [2008]). Incoming ($S\downarrow$) and reflected ($S\uparrow$) short-wave radiation were determined with upward and downward looking Kipp & Zonen CM 22 (Delft, Netherlands) pyranometers. Incoming ($L\downarrow$) and outgoing (L$\uparrow$) long-wave radiation were measured with two Eppley (Newport, United States) pyrgeometers. Air temperature (T_{air}) and relative humidity (rh), as well as wind velocity (v) and direction were measured with an Automatic Weather Station (AWS, Thies-Klima, Göttingen, Germany) in 2-m height above the snow surface. All parameters were measured in 10-s intervals and averaged to 5-min values by the data logger.

[20] All sensors were visited at least once a day in order to clean and readjust them, if necessary. During station setup, the snow underneath and around the station was as little disturbed as possible in order to preserve the original, homogeneous surface and snowpack. From the ratio of incoming and reflected short-wave radiation, surface albedo was calculated, neglecting periods of low Sun elevation with $S\downarrow < 100$ W m^{-2} to avoid high inaccuracies through division of small values.

[21] Additional meteorological measurements were performed at FY2 (map in the work of *Hellmer et al.* [2008]) by the FIMR station [*Vihma et al.*, 2009]. The AWI and FIMR stations had very similar instrumentation, except that additional measurements of turbulent fluxes of momentum and heat were performed at the FIMR station. Both stations were set up above different snow regimes to enable studies of the influence of different snow regimes on the surface energy balance. Comparing incoming short-wave radiation, both stations show an accuracy of approximately 3% [*Vihma et al.*, 2009]. Furthermore, we use the FIMR data set for comparison of different radiation fluxes and surface albedo.

[22] From the presented meteorological measurements at the AWI site, sensible (q_s) and latent (q_l) heat fluxes were derived using the bulk aerodynamic approach [*Launiainen and Cheng*, 1995]. The total surface energy balance (Q) at the air and snow interface was computed as

$$Q = Q_s + Q_L + Q_T, \tag{2}$$

$Q_S = S\downarrow - S\uparrow$ denotes net short-wave, $Q_L = L\downarrow - L\uparrow$ denotes net long-wave radiation,and $Q_T = q_s + q_l$ denotes turbulent heat fluxes. All net fluxes are defined positive downward, representing an energy input into the snow. On the basis of the mean surface energy balance a potential melt rate can be computed using the latent heat of snowmelt (0.3335 MJ kg^{-1}) and a mean snow and ice density of 300 kg m^{-3} and 910 kg m^{-3}, respectively. This assumes that all energy is used up for melting.

[23] Ocean heat flux was measured by *McPhee* [2008]. However, it is neglected here for the net heat flux into the snow, because upward heat conduction through the ice was very low, the temperature minimum was within the sea ice, and hardly any basal sea-ice melt was observed [*Haas et al.*, 2008a; *McPhee*, 2008]. The positive heat flux into the ice was consumed for internal warming (= internal melting) and change of porosity, but not for thickness changes (= basal melting) [*Haas et al.*, 2008a].

3. Results

3.1. Meteorological Conditions, Surface Albedo, and Atmospheric Heat Flux

[24] Meteorological conditions during the drift were dominated by long periods of overcast conditions and prevailing winds from north to east with a strength of 1 to 5 m s^{-1} (Figure 3f) [see also *Bareiss and Görgen*, 2008]. Stronger winds with velocities up to 11 m s^{-1} mostly originating from northwest to north and were generally warmer, but they occurred only during three phases (from 30 November to 2 December, on 20 December, and from

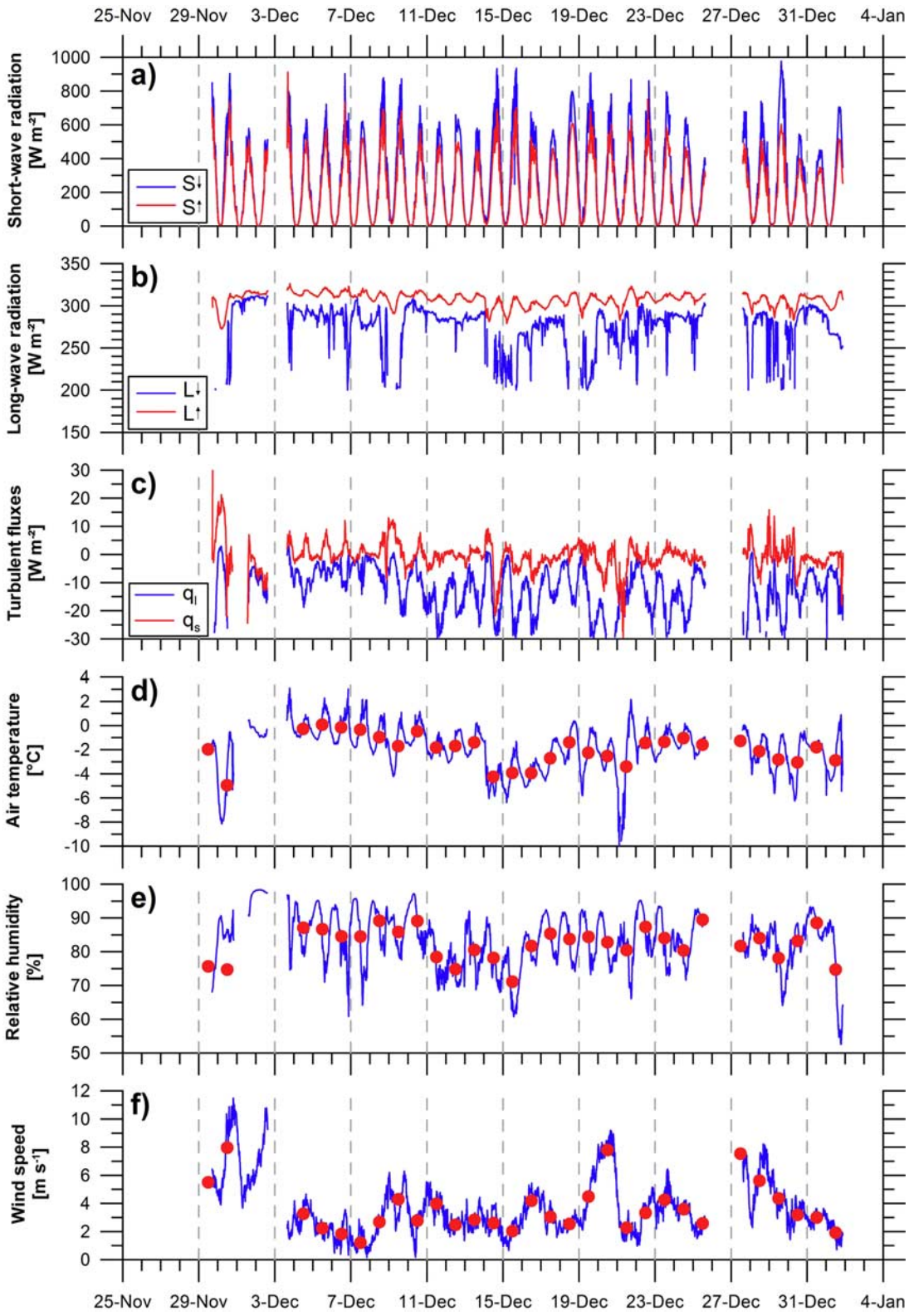

Figure 2. Radiation and weather conditions during the ISPOL drift (5-min intervals). (a) Incoming (S↓, blue) and reflected (S↑, red) short-wave radiation, (b) incoming (L↓, blue) and outgoing (L↑, red) long-wave radiation, (c) latent (q_l, blue) and sensible (q_s, red) heat flux, (d) air temperature, (e) relative humidity, and (f) wind velocity. Measurements were performed on FY1 until 12 December and on FY2 after 12 December. Missing data are caused by relocation of the station after the two floe breakups. Daily means of energy balance components (Figures 2a, 2b, and 2c) are shown in Figure 3; those for weather station data are shown here as red dots (Figures 2d, 2e, and 2f).

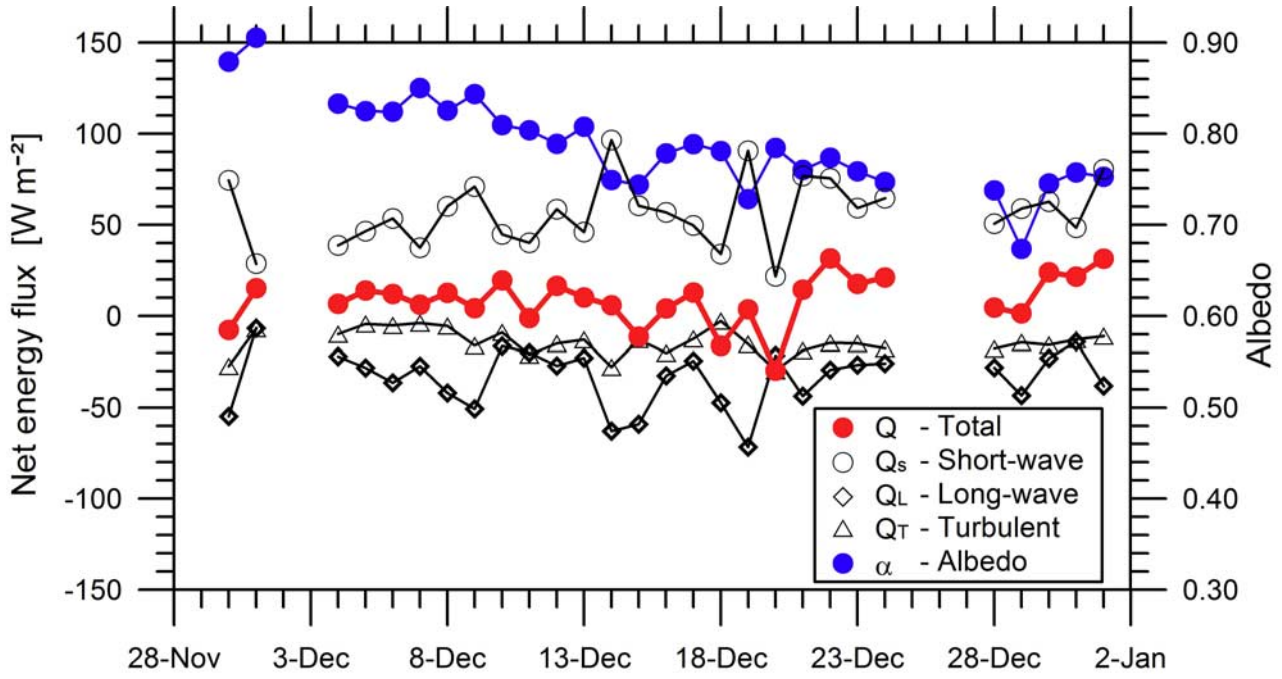

Figure 3. Daily means of net energy fluxes (left axis, red and black lines) and surface albedo (right axis, blue line). Missing data are due to station relocations. Full-resolution data sets of Q_S, Q_L, and Q_T are shown in Figure 2, and those of albedo are shown in Figure 4.

27 to 28 December). Winds directed from the west, from the region of the Antarctic Peninsula, were rare.

[25] Air temperatures were mostly between −3.0 and 0.0°C and fell below −5.0°C only during a few cases of cold air advection and cases of surface inversion generated by radiative cooling in clear and calm nights (Figure 2e). Mean air temperature was significantly higher during the first 2 weeks of December (−0.9°C) than during the subsequent 3 weeks (−2.4°C). More detailed analyses of meteorological conditions are published by *Bareiss and Görgen* [2008], *Bock et al.* [2007], and *Vihma et al.* [2009].

[26] Incoming short-wave radiation decreased close to 0 W m^{-2} during every night (Figure 2a). Maximum incoming short-wave radiation exceeded 900 W m^{-2} on clear-sky days and amounted to 400 to 600 W m^{-2} under overcast conditions. As a consequence, net short-wave radiation was around 200 W m^{-2} during daytime and averaged to 56 W m^{-2} over the whole observation period (Figure 3). Outgoing long-wave radiation varied only little over the entire observation period (Figure 2b). This is because of its dependence on the snow surface temperature, which varied only slightly diurnally, and was close to the melting point both on thick and on thin snow (compare to Figure 7). As a consequence, changes of net long-wave radiation were dominated by the more variable incoming long-wave radiation. Q_L had highest values (−15 to −10 W m^{-2}) during overcast conditions and decreased to −90 W m^{-2} during several short clear-sky periods (Figure 3). Mean net long-wave radiation was −34 W m^{-2}. Turbulent fluxes were strongly negative with a mean value of −14 W m^{-2} over the whole observation period (Figures 2c and 3), consisting of −12.8 and −1.4 W m^{-2} for latent and sensible heat, respectively. Detailed studies on turbulent fluxes were presented by *Vihma et al.* [2009]. Relative humidity mainly varied between 80 and 95% (Figure 2e).

[27] Figure 3 shows daily averages of net heat fluxes as well as surface albedo, but includes only days for which a full 24-h data set could be obtained. Short-wave radiation led to a net energy flux into the snow whereas long-wave radiation and turbulent fluxes led to energy loss into the atmosphere, over the whole drift. The resulting net heat flux to the snow (Q) showed phases of positive and negative balances before 21 December and was continuously positive afterward. The overall mean Q during ISPOL was 8 W m^{-2}, consisting of 56 W m^{-2} net short-wave radiation (Q_S), −34 W m^{-2} net long-wave radiation (Q_L), and −14 W m^{-2} net turbulent heat fluxes (Q_T). The energy input into the snow is equivalent to 0.68 MJ m^{-2} d^{-1} (or 21 MJ m^{-2} in 31 days) or a potential snowmelt rate of 0.68 cm d^{-2} (21.1 cm of snow in 1 month). The mean atmospheric energy flux was approximately half of the mean ocean heat flux of 15 W m^{-2} (46.3 MJ m^{-2} in 31 days), as measured by *McPhee* [2008].

[28] For comparison, the Q at the FIMR station was only 3 W m^{-2}, consisting of 52 W m^{-2} (Q_S), −29 W m^{-2} (Q_L), and −20 W m^{-2} (Q_T) [*Vihma et al.*, 2009]. This is equivalent to 0.25 MJ m^{-2} d^{-1} (7.8 MJ m^{-2} in 31 days) or a potential snowmelt rate of 0.25 cm d^{-1} (7.8 cm of snow in 1 month). Both data sets show significant differences in all components of the surface energy balance. These differences may indicate different snow regimes at the stations, which were supported by a more grayish visual appearance of the surface at FIMR. However, on the other hand, the measured variations may only be the result of observational uncertainties resulting from the general difficulties of performing energy balance measurements during summer, different data processing, and partially different registration periods due to station relocations. In any case, both data sets

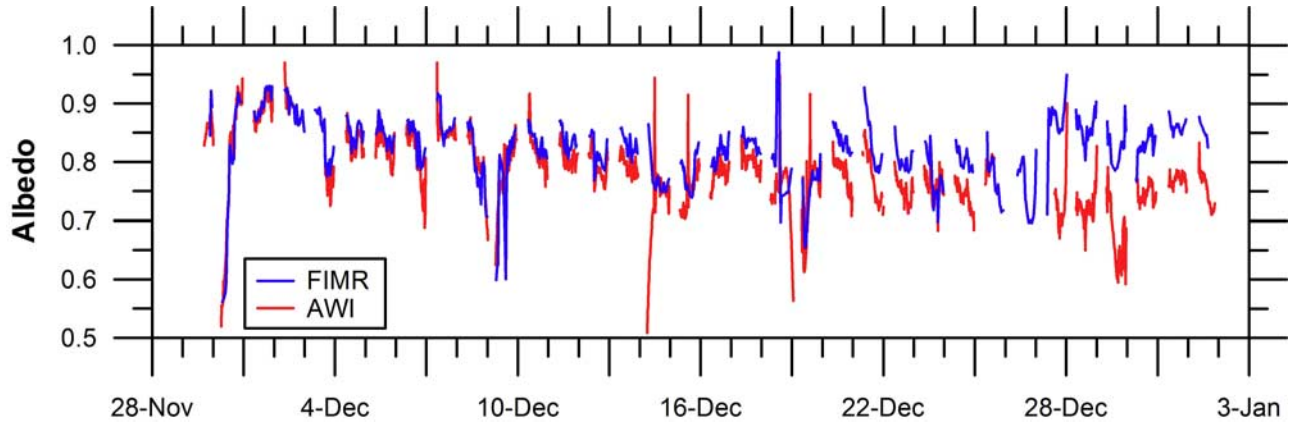

Figure 4. Surface albedo from continuous (5-min intervals) radiation measurements on different sites. Both stations were located over different snow regimes. Missing data are due to station relocations, and incoming short-wave radiation values below 100 W m^{-2} were filtered out. Daily means of albedo at the AWI station are shown in Figure 3. Additional information about Finnish Institute of Marine Research (FIMR) albedo may be found in the work of *Vihma et al.* [2009].

show that meteorological measurements over warm snow surfaces are very difficult and erroneous, even if they are performed with high accuracy and caution. Hence, measurements of snow properties and meteorological parameters should be used for cross validations. Comparisons of both data sets, e.g., regarding surface temperatures or observed changes, can help to increase the reliability of both data sets.

[29] Broadband surface albedo decreased during the observation period from a daily mean of 0.86 to 0.66 on 27 December, when new snow fall caused an increase to 0.75 (Figure 3). In general, surface albedo of different snow regimes decreased moderately by 0.10 to 0.20, but did not trigger strong albedo feedbacks, which would have induced a more rapid, stronger albedo decrease [e.g., *Curry et al.*, 2001; *Holland et al.*, 2001; *Maykut and Untersteiner*, 1971; *Perovich et al.*, 2002, 2008]. Figure 4 compares broadband albedo of different snow regimes, measured at the two radiation stations (FIMR and AWI). The AWI station was operated over initially 0.32-m-thick first-year snow, whereas the FIMR station obtained readings from 0.45- to 0.50-m-thick second-year snow. In the beginning of observations the albedo of the thicker snow (FY2, FIMR) was only about 0.02 higher than that of the thinner snow (FY1, AWI). This difference increased with time to 0.06 on 25 December, because of different snow metamorphism on both FYI sites. But surface albedo differed by 0.10 between the stations from 27 December onward, after the AWI station had to be relocated to a thinner, more metamorphic, and grayish appearing spot on FY2. This explains at least some of the differences in net heat fluxes between AWI and FIMR stations. Further analysis of FIMR albedo data is discussed by *Vihma et al.* [2009].

3.2. Snow Thickness and Stratigraphy

[30] We distinguish two snow regimes: Thicker snow on SYI and thinner snow on FYI. Both snow regimes persisted throughout the observation period, and their thickness decreased by no more than 20 cm, as shown in detail below. Freeboard was negative on most of the measurement sites. However, extensive flooding was primarily observed on the FYI sites (Figure 6). Figure 5 shows time series of snow thickness on two FYI and SYI sites of the ISPOL floe. On

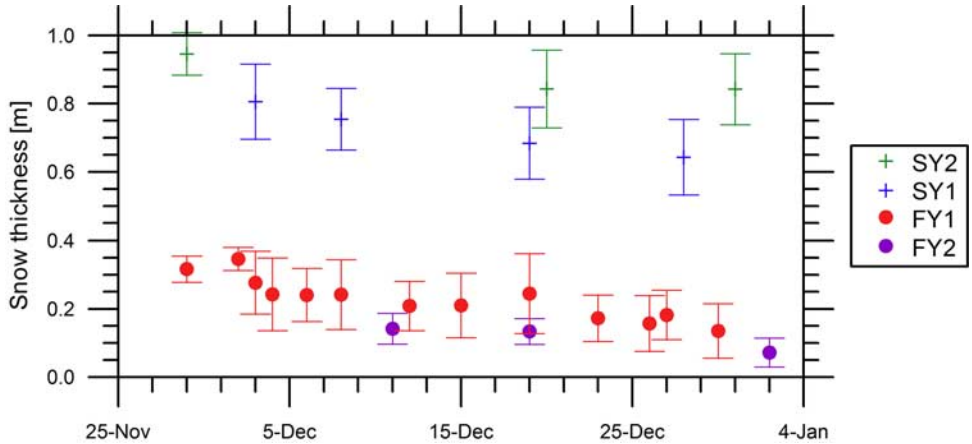

Figure 5. Mean snow thickness (and standard deviation) of different sites (for nomenclature, see text and *Hellmer et al.* [2008]). Measurements on 19, 28, and 31 December were performed with a metal pole instead of a wooden ruler.

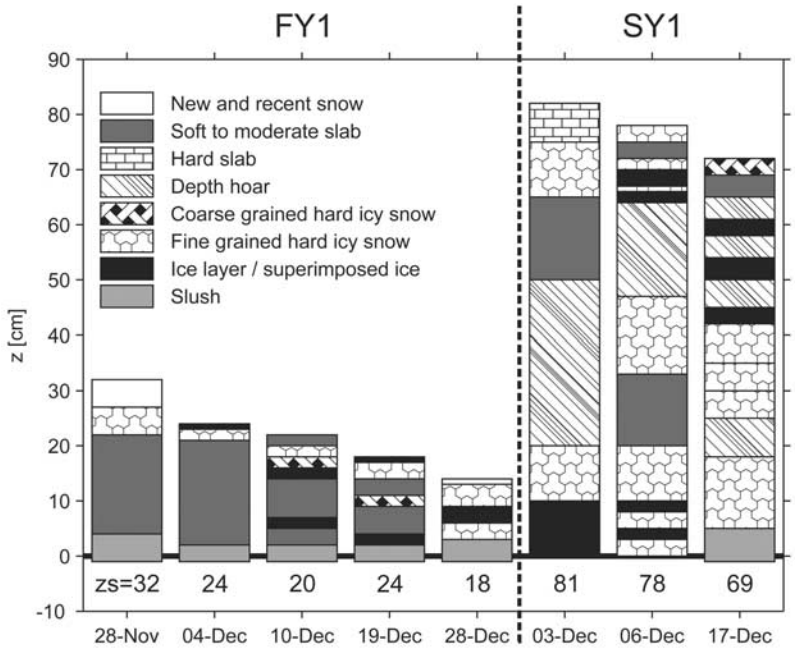

Figure 6. Snow stratigraphy on FY1 (left, 5 days) and SY1 (right, 3 days): $z = 0$ demarcates water level; snowpacks with positive freeboard are aligned at $z = 0$. Mean snow thickness (z_s) from stake measurements along a 50-m profile are given above the dates in centimeters. This depth usually deviates slightly from the local snow depth at the snow pit location, where stratigraphy was recorded.

FY1, snow thickness decreased from 31.7 ± 3.9 cm (29 November) to 13.7 ± 8.0 cm (30 December). This corresponds to a mean decrease of 0.51 cm d^{-1} (R^2 = 0.79, number of observations n = 13). This includes new snow events on 2 and 27 December, when snow thickness increased temporarily. Snow thickness on FY2 decreased by only 0.33 cm d^{-1} (R^2 = 0.93, n = 3) from an initial thickness of 14.0 ± 4.5 cm. But the absolute thinning amounted to 7.0 cm, the same as on FY1.

[31] Snow on SY2 reduced from 9 to 20 December by 10.3 cm from 94.6 ± 6.2 to 83.3 ± 10.4 cm. This corresponds to a mean thinning rate of 0.49 cm d^{-1} (n = 2). The last thickness measurement on this patch is only partly comparable with all previous values, because all measurements were made with a metal instead of a wooden ruler. Although this results in a slightly larger snow thickness reading, it did become necessary because several ice layers had formed in the snow in the meantime, which were not anymore penetrable with the wooden stick. On SY1, snow thickness decreased from 81.0 ± 11.0 to 64.0 ± 11.0 cm by 0.64 cm d^{-1} (R^2 = 0.89, n = 4).

[32] The observed snow thinning lay within the range of potential snowmelt rates calculated from the mean surface energy balances at the AWI and FIMR stations (0.68 cm d^{-1} and 0.25 cm d^{-1}, respectively). This calculation assumes that all energy is consumed by melting alone, disregarding energy contributions to warming of snow and ice. In fact, the latter consumes a major fraction of atmospheric energy input into the snow because of the large heat capacity of sea ice at temperatures close to melting [*Yen et al.*, 1991]. On the basis of the results by *Haas et al.* [2008a], showing that the temperature minimum was always within the ice, it is very likely that atmospheric heat fluxes significantly contribute to warming of sea ice, at least in the uppermost centimeters.

[33] Since no quantitative measurements of snow accumulation were performed during ISPOL, the only estimate of new snow accumulation can be derived from snow thickness measurements on FY1, where the most extensive time series of snow thickness was obtained. A combination of these data with qualitative meteorological observations [*Bock et al.*, 2007] shows two major snow fall events. The first occurred between 28 November and 2 December and increased snow thickness by 6.8 cm (Figure 5). The second occurred between 26 and 27 December and added 1.3 cm of snow.

[34] Snow stratigraphy differed significantly for first-year and second-year snow, as shown for FY1 and SY1 in Figure 6. Over the entire observation period, first-year snow mainly consisted of soft to moderate slabs (59%). Fine grained hard icy snow (20%) and ice layers were of minor importance, but appeared more frequently in the course of time. Depth hoar was only found in a single snow pit on 2 December. Second-year snow consisted of fine-grained, hard icy snow (38%) and depth hoar (30%). Alternating layers of ice lenses and depth hoar were a characteristic stratigraphy toward the end of the observation period in thick snow. Although temperatures at the snow and ice interface where never close to melting (see below), and no continuous or episodic formation of superimposed ice was observed directly, there was a 2-cm-thick layer of superimposed ice in the snow pit above slush on FY1 on 19 December. Likewise, a 10-cm-thick layer of superimposed ice was found as a basal ice layer underneath the thick snow cover of SY1 on 3 December, but the formation of this layer is difficult to date and explain, since it formed before the observations started.

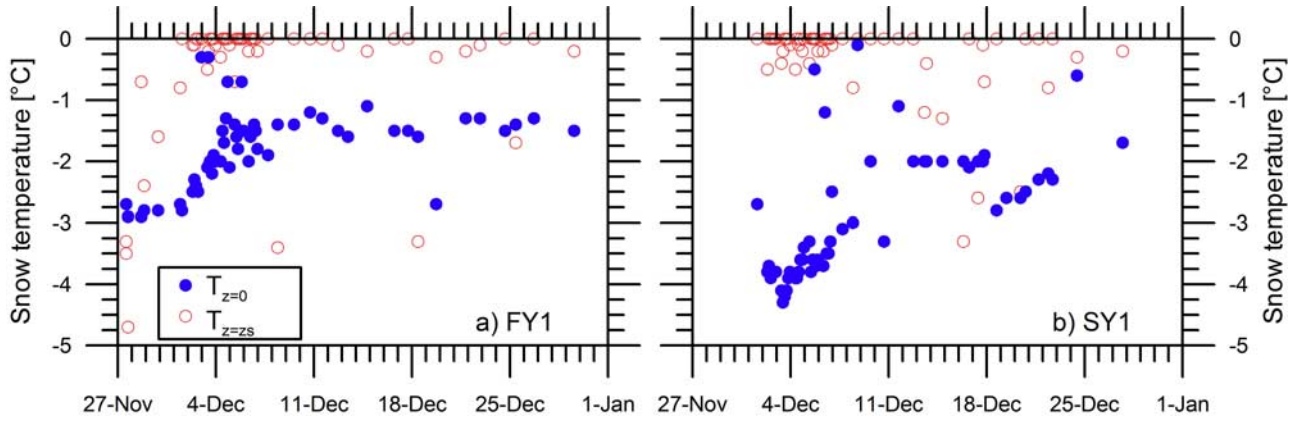

Figure 7. Temperature of snow at its surface ($T_{z=zs}$, red circles) and at the snow-ice interface ($T_{z=0}$, blue dots) of all measured temperature profiles on (a) FY1 and (b) SY1. Until 7 December, measurements were performed every 3 h to evaluate diurnal changes; afterward daily measurements were taken around time of the maximum temperature in the snow cover (1700 local time) to observe daily variations. The legend refers to both Figures 7a and 7b.

[35] We assume that most depth hoar crystals formed during autumn and winter, before our observations, because (1) the fraction of depth hoar was highest at the beginning of the observations (Figure 6) and (2) all measured temperature gradients were much higher than the threshold for depth hoar formation of -25 °C m^{-1}.

[36] Mean snow grain sizes were between 1 and 2 mm at the beginning and between 3 and 4 mm toward the end of the observation period in first-year snow. Mean grain sizes of second-year snow were very similar, but larger (>5 mm) depth hoar crystals were observed frequently, too.

3.3. Snow Temperature and Temperature Gradients

[37] During the beginning of observations, snow surface temperatures possessed a strong diurnal cycle, which diminished for deeper snow layers and when the snow reached the melting temperature. Surface temperatures were generally highest at 1300 LT (1700 UTC) and lowest at 0400 LT (0800 UTC), in agreement with the diurnal cycles of radiation components and air temperature (Figure 2). *Vihma et al.* [2009] derived a diurnal cycle of surface temperatures of 1.6°C from radiation measurements for the entire observation period.

[38] Snow surface temperature repeatedly reached the melting point (0.0°C) on FY1 and SY1 already from 1 December onward (Figure 7), when the phase of low air temperatures ended (Figure 2d). The 0.0°C isotherm depth varied between 5 and 10 cm below surface. Surface temperature minima varied between -1.0 and -8.0°C, with lowest temperatures during clear-sky conditions (Figure 2b).

[39] The snow-ice interface did not reach 0.0°C during ISPOL, neither under thin snow on FYI (e.g., FY1) nor under thick snow on SYI (e.g., SY1), as shown in Figure 7. Only 6 of 56 temperature profiles (all on SY1) had a snow-ice interface temperature T ($z = 0$) above -1.8°C (Figure 7a), which can be explained through flooding.

[40] Snow and upper sea-ice temperatures were higher in thinner snow on FYI (e.g., FY1) than in thicker snow on SYI (e.g., SY1) at any given time (Figure 7). In the beginning of December, upper sea-ice temperatures were above -3.0 and -4.0°C on FY1 and SY1, respectively. They increased steadily within the first week and approached a nearly constant temperature of -1.5 ± 0.3 and -2.1 ± 0.5°C on FY1 and SY1, respectively.

[41] On the basis of the vertical temperature profiles from Figure 7, temperature gradients in the total snow cover ($(T_{z=zs} - T_{z=0})/z_s$, Figures 8a and 8c) and in the topmost 25% of the snow cover ($(T_{z=zs} - T_{z=0.75 \times zs})/(0.25 \times z_s)$, Figures 8b and 8d) were calculated. Results show mostly positive temperature gradients in agreement with higher snow surface and lower snow-ice interface temperatures. Highest temperature gradients, with values up to 10°C m^{-1}, were present in the beginning of the observation period, when the snow-ice interface was coldest (Figure 7). Corresponding to increasing snow-ice interface temperatures, temperature gradients strongly decreased until 9 December. The snow became nearly isothermal in the topmost 25%, as temperature gradients are close to 0°C m^{-1}. On FY2, the snow was thin and very icy. Hence, its heat conductivity was probably higher, leading to a nearly isothermal snow cover (Figure 8a). The higher scatter of surface temperature gradients (Figure 8b) might be explained with low snow thicknesses, resulting in higher inaccuracies during computation. Surface (topmost 25%) temperature gradients were generally smaller than those over the whole snow cover. This indicates a significant absorption of short-wave radiation in the topmost snow layers, which led to enhanced surface warming, but was not strong enough to induce strong snowmeltwater production. Note that most measurements were taken during the temperature maximum in the snow cover around 1700 LT, such that night hour temperature gradients may be assumed to be lower and even negative (Figure 2d).

3.4. Snow Density and Mass Balance

[42] Vertically averaged snow densities were measured with the Snow Fork and volumetrically (Figure 9). For all days, when both methods were applied, these averages agree within 34.2 kg m^{-3}, except the last measurement on SY1 when Snow Fork densities are significantly lower. This results probably from the distinct stratification of the snowpack, because in layered and icy snow, the assumption

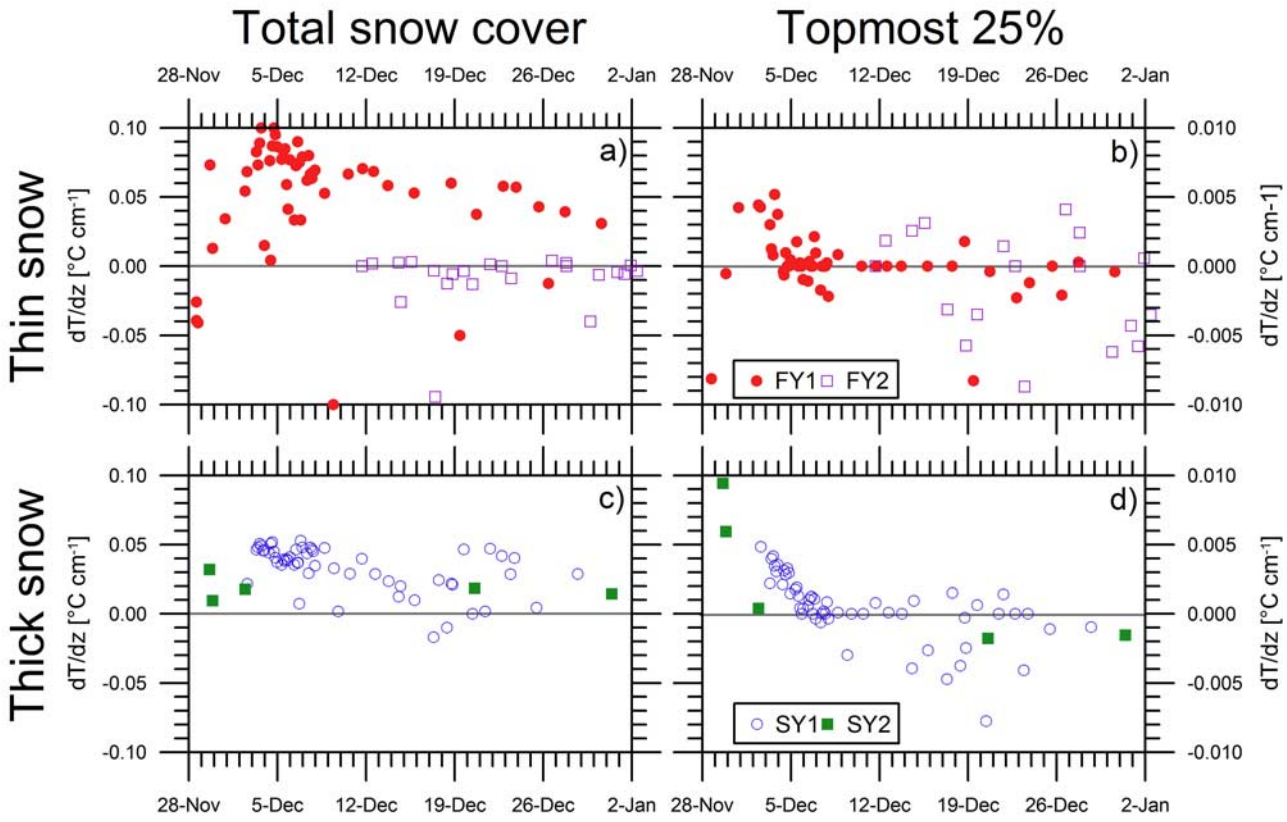

Figure 8. Snow temperature gradients on different sites. (a and c) Mean gradient between snow surface ($z = z_s$) and snow-ice interface ($z = 0$) for (Figure 8a) first-year and (Figure 8c) second-year snow. (b and d) Mean gradient within the topmost 25% of the snow thickness for (Figure 8b) first-year and (Figure 8d) second-year snow. Note that the y axis scale is 1 order of magnitude smaller for surface temperature gradients (Figures 8b and 8d) than for the entire snow cover (Figures 8a and 8c).

of a homogeneous snowpack around the Snow Fork is not anymore valid.

[43] On FY1, both methods give consistent results. Snow density increased from 250 kg m^{-3} (until 6 December) to 385 kg m^{-3} (after 25 December) by more than 50%. This increase in density was mainly due to destructive metamorphism, increasing snow wetness, and compaction through weight and wind. Mean density was 282 ± 83 kg m^{-3}. In contrast, on SY1, both methods show different results. Snow Fork mean density increased from 332 ± 65 kg m^{-3} (until 4 December) to 441 kg m^{-3} (9 December), before it decreases to densities even below 200 kg m^{-3} at the end of observations. These results do not represent the temporal evolution of mean density, but are biased through

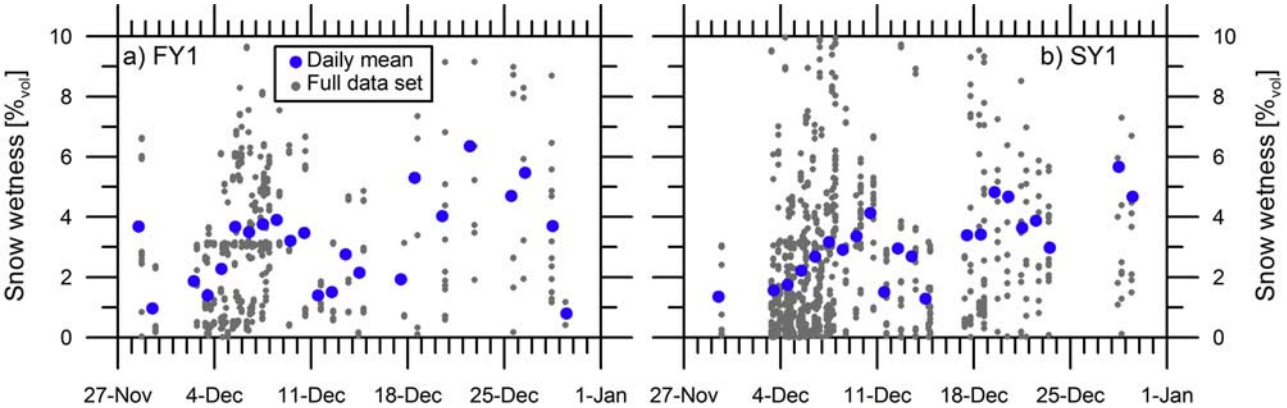

Figure 9. Vertically averaged snow density, measured in snow pits with the Snow Fork and a volumetric method on (a) FY1 and (b) SY1. The number of measurements per snow pit ranges from 1 to 11, depending on snow thickness and stratigraphy. The legend refers to both Figures 9a and 9b.

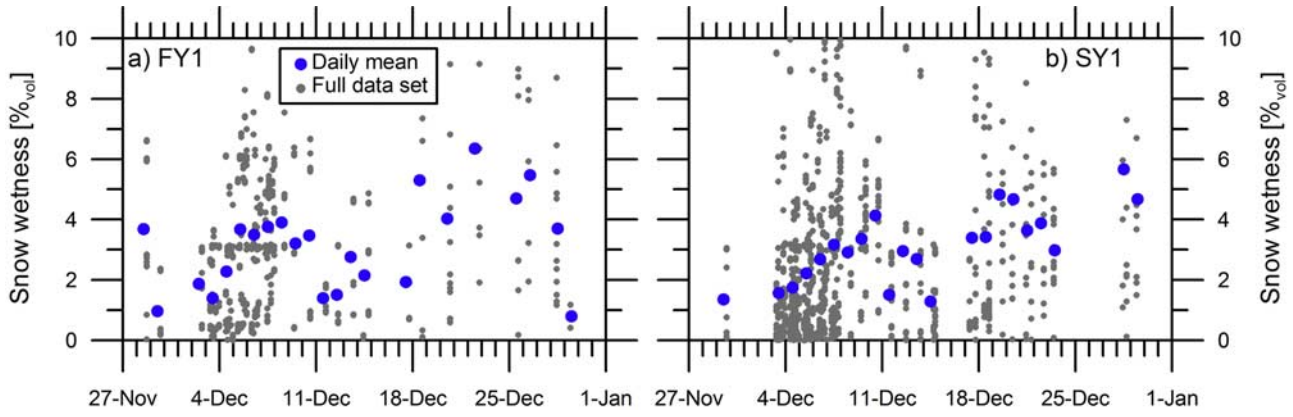

Figure 10. Vertical averages of snow wetness from Snow Fork measurements on (a) FY1 and (b) SY1. For better readability, single measurements >10%$_{vol}$ (38 of 1478) are not shown, and the legend refers to both Figures 10a and 10b.

methodical shortcomings. Increasing stratification of the snow affects the reliability of snow fork mean densities. Icy layers do not give valid measurements, hence vertical averages are dominated by layers of lower density, like depth hoar (Figure 6), which still can be adequately sampled. The two volumetric measurements describe an increase of density by 12% from 337 (5 December) to 376 kg m^{-3} (28 December) with a mean density of 356.5 kg m^{-3}. Hence mean density of SYS was significantly larger than that of FYS despite the higher fraction of depth hoar in SYS.

[44] Snow mass loss dm (equation (1)) amounted to 27.3 kg m^{-2} on FY1 and 32.4 kg m^{-2} on SY1, respectively (Table 1). Compared to the net energy flux of 0.68 MJ m^{-2} d^{-1}, only 43 to 63% of the available energy would be needed to melt these snow masses. Considering the rather high spatial variability of snow thickness and density, both snow types show very similar mass losses. From the high average turbulent heat flux and the vertical snow temperature profiles, it may be concluded that evaporation significantly contributed to the total snow mass decrease. To quantify this hypothesis, numerical snow cover simulations were performed on the basis of the study by *Nicolaus et al.* [2006], using the one-dimensional snow model SNTHERM [*Jordan*, 1991]. *Nicolaus et al.* [2006] use the initial snow conditions from FY1 and the meteorological observations as presented here. Their results show that 36 (FY1) to 51% (SY1) of the total snow mass loss is due to evaporation. On the ISPOL floe, all meltwater remained within the snow cover and contributed to superimposed ice formation (see below), which confirms earlier results from field measurements [*Willmes et al.*, 2006] and numerical simulations [*Nicolaus et al.*, 2006].

3.5. Snow Salinity

[45] Snow salinity was below the detection level of the salinometer in all FYS and SYS samples. Only in the lowermost 0- to 5-cm, elevated values of up to 1.9 were occasionally measured. This is in contrast to earlier observations by *Massom et al.* [2001] who show salinities above 10 to be a common feature in the bottommost 0.1-m snow layers on Antarctic sea ice during winter. *Massom et al.* [2001] explain increased snow salinities on sea ice with capillary suction of brine and/or the incorporation of frost flowers, which are most pronounced on young and thin ice. The question arises if downward salt transport did occur in the snow during possible warming events already before the ISPOL observation period, reducing prior higher snow salinities.

3.6. Snow Wetness and Liquid Water Transport Through Snow

[46] Vertically averaged snow wetness slowly increased from the beginning of the observations until 11 December on first-year and second-year snow, but remained below 4%$_{vol}$ (Figure 10). After 15 December a significant increase of snow wetness was determined for both sites. Mean daily snow wetness was 4.3%$_{vol}$ in first-year snow and 4.1%$_{vol}$ in second-year snow. Additionally, snow-wetness variability increased in both snow cover types, but is most prominent for thinner snow (FY1). *Willmes et al.* [2009a] discuss that this increase in variability accompanied an amplification of the diurnal cycle of brightness temperature and increasing melt-freeze cycles.

[47] Figure 11b shows a qualitative example of a vertical snow profile where the tracer concentration maximum can be clearly seen at the snow-ice interface, indicating that significant downward percolation of the tracer has occurred. A typical vertical thick section of metamorphic snow, superimposed ice, and sea ice obtained from the same snow pit is shown in Figure 11c.

[48] Figure 12 presents results of the tracer experiments performed on FY2 from 26 December 2004 to 2 January 2005. SR concentrations are given relative to maximum SR concentration within the particular profile, in order to avoid biases due to spatially irregular initialization or effects due to SR decay from exposure to solar irradiation. Figures 12a and 12c show that 5 h after initialization most of the SR was still found in the topmost 2 cm, and only small fractions had percolated to a depth of 7 cm. This corresponds to a mean percolation velocity of 1.2 cm h^{-1} at the beginning of the experiments. Similar transport velocities of more than 1.1 cm h^{-1} (>26 cm d^{-1}) were reached during the first day, when most of the SR passed the whole snow cover of 29-cm thickness in less than 27 h (Figures 12b and 12d). Because of rather long time intervals between single samplings, it was not possible to detect the moment when the

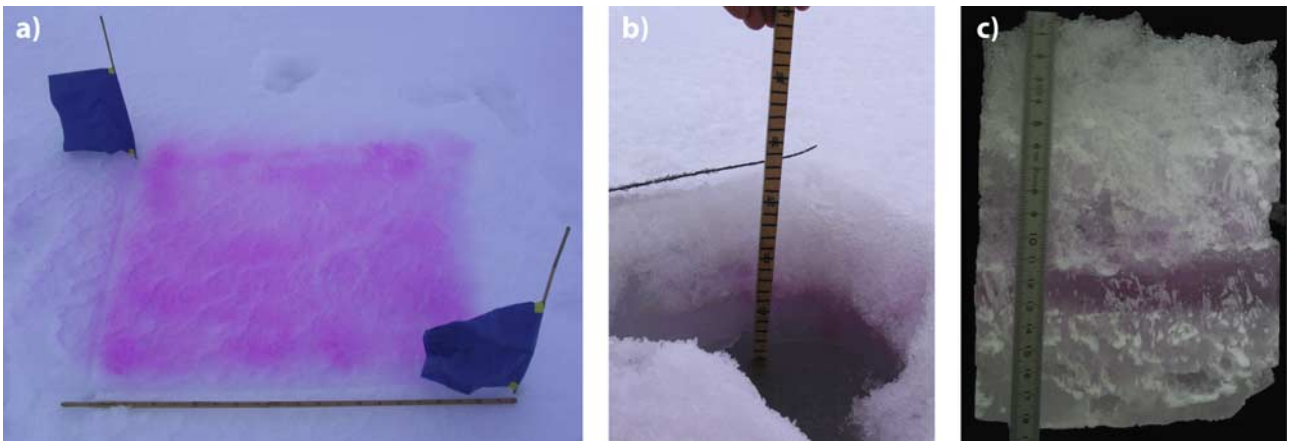

Figure 11. Photographs of tracer experiments with Sulforhodamin-B. (a) Snow surface immediately after the tracer (pink color) was sprayed homogenously over a 1 × 1-m snow surface, marked by flags and a 1.10-m long ruler stick. (b) Snow pit 27 h after injection (for data, see Figure 12b). (c) Vertical thick section of a snow and ice sample (27 h after injection; for data, see Figure 12b). All scales are in centimeters.

maximum concentration reached the topmost (see stratigraphies in Figure 12) snow and ice interface. After 3 days (78 h) the maximum concentration is still at the ice surface, but the tracer front had progressed further into and through the uppermost ice layers (Figures 12a–12d). All experiments show concentration maxima in the ice layers within 2 to 6 days, but only low concentrations at the ice bottom or in the slush underneath.

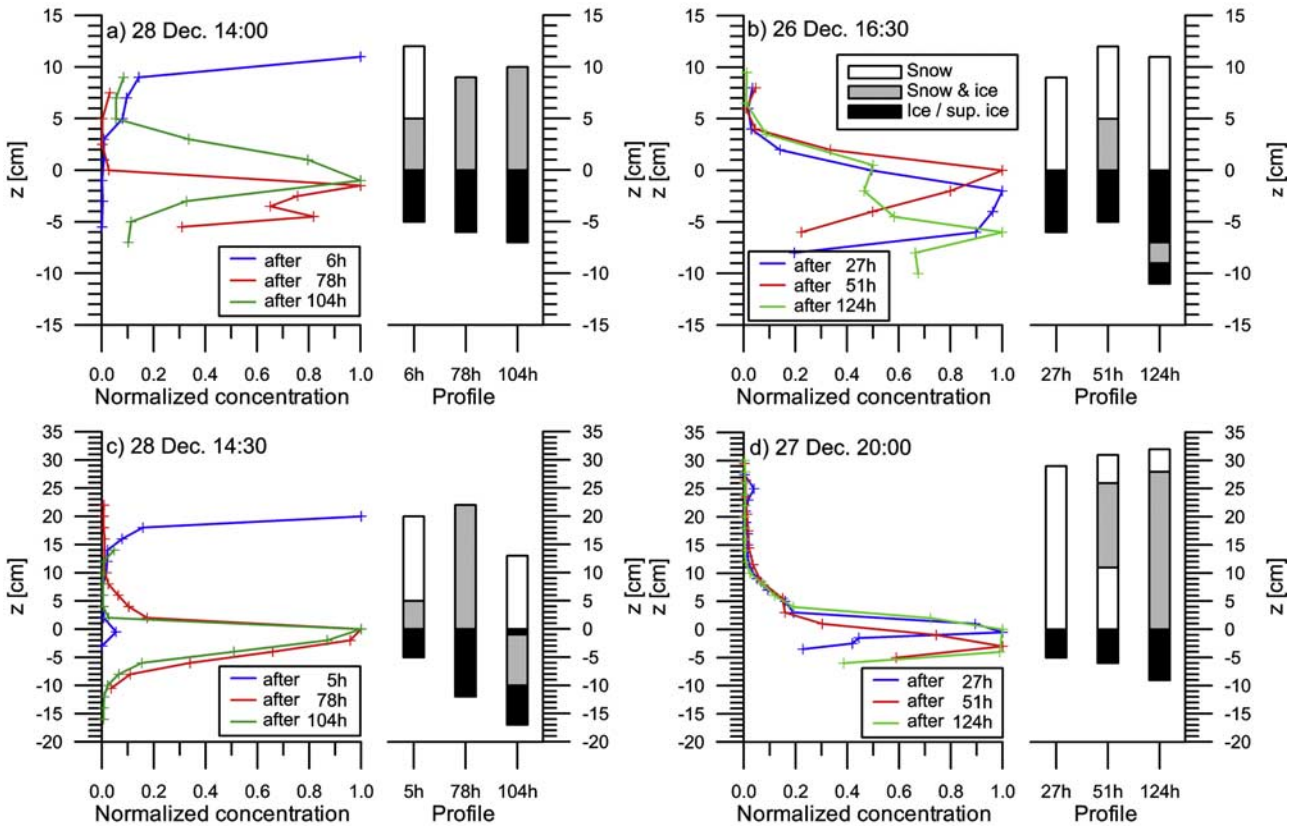

Figure 12. Sulforhodamin-B (color tracer) concentration from surface cores of snow and ice layers in different time intervals (5 to 124 h) after injection (on FY2 between 26 and 28 December). Profiles in (a and b) thinner and (c and d) thicker snow. All concentrations are normalized to the maximum value of the according surface core, and $z = 0$ denotes the surface of the uppermost ice layer within the core. All surface cores reach from the snow surface down to the surface of the slush layer (on top of the sea ice). Given dates and times are those of the injection.

Figure 13. Photographs of vertical thick sections from surface cores comprising metamorphic snow, ice layers, and superimposed ice: (a) 30 December, FY1, (b) 20 December, SY2, and (c) 30 December, FY1. All scales are in centimeters. Note slightly different scales in Figures 13a–13c.

3.7. Superimposed Ice Occurrence

[49] As presented above, the fraction of ice layers in the snow cover increased from the first half of December onward (Figure 6). These ice layers were mostly discontinuous and horizontally variable on a scale of decimeters (Figure 13). Mean ice layer thickness was below 2 cm, but ranged up to 10 cm for some ice lenses within second-year snow or at the snow-ice interface. The first superimposed ice was found underneath first-year snow on FY1 on 11 December. It had formed on top of a slush layer, was up to 2 cm thick and mostly unconsolidated, which made its sampling rather difficult. However, even after this first detection, superimposed ice formation varied highly laterally within a few decimeters (Figure 13b), and no gradual increase in the amount or thickness could be reliably observed. Hence superimposed ice occurred only in one snow stratigraphy profile on 19 December (Figure 6). During the course of time, superimposed ice thickness and consolidation did not change significantly, and it was not possible to create a reliable time series of superimposed ice thickness and distribution.

[50] Figure 13c shows the vertical (from top to bottom) layering of metamorphic snow, internal ice layer with air bubbles, metamorphic and highly compacted snow, and superimposed ice, as it was frequently found on the ISPOL floe at the end of observation period. The surface of superimposed ice (snow-ice interface) was very rough on centimeter scale (photograph in Figure 13b). In contrast, the bottom of the superimposed ice layer is very flat, as it has formed on a slush layer. These findings are in agreement with earlier observations of superimposed ice on Antarctic sea ice [*Haas et al.*, 2001].

[51] In contrast to the subtle changes on the ISPOL floe, snow metamorphism and superimposed ice formation developed very differently on the FIMR floe, initially 100 km north of the ISPOL floe (Figure 1). On the FIMR floe, snow thickness decreased from 27.7 ± 10.1 cm to 9.6 ± 5.3 cm, and a 5-cm thick layer of consolidated superimposed ice had formed uniformly over large areas (observed along a 50-m-long snow-thickness profile) on top of 17-cm slush within the 23 days between observations on 9 December and 1 January. On 1 January, the underlying sea ice was 0.50 ± 0.04 m thick (very uneven bottom) and highly porous. Its topmost centimeters showed a honeycomb structure with pronounced brine channels underneath, indicating strong internal and basal melting. Ice thickness was not measured during the first visit.

[52] Two days after leaving the ISPOL floe (4 January 2005), two floes (EDGE, Figure 1) were visited at the ice edge at 66.2°S, 55.5°W, 120 km north of the end position of the ISPOL drift. On both floes a distinct layer of superimposed ice had formed above a narrow gap layer. Snow cover was 9 and 22 cm thick, highly metamorphic, and consisted of very coarse grains with diameters of 5 mm to more than 10 mm.

4. Discussion

4.1. Differences and Similarities of Snow on FYI and SYI

[53] Our results show a large spatial and regional variability of snow properties in the western Weddell Sea, as a consequence of the variety of underlying ice types and atmospheric processes acting on the snow during its evolution. This high variability, together with methodical difficulties, makes general conclusions very difficult, as already found during earlier studies on snow on Antarctic sea ice [*Massom et al.*, 1997; *Morris and Jeffries*, 2001; *Sturm et al.*, 1998].

[54] However, it was possible to find general and characteristic differences of physical properties of snow on FYI and SYI. These were in particular different snow thicknesses, basal and internal snow temperatures, and the occurrence of depth hoar. Differences in snow thickness (on level ice) resulted from different accumulation periods and histories, because the history of the underlying sea ice was different. It originated from different regions and was of different age. Snow temperatures were lower on SYI, because the SYI was thicker and colder and acted as a cooling reservoir for the snow. Additionally the larger snow thickness results in a stronger insulation toward the warmer atmosphere. The fraction of depth hoar was larger on SYI than on FYI. Explanations therefore might be that (1) the snow on FYI accumulated too late to experience high temperature gradients due to low air temperatures and

(2) the snow on SYI contained more moisture at the end of the previous summer and autumn, which might have supported depth hoar formation. Observations of decreasing fractions of depth hoar in snow on SYI complement earlier results, e.g., by *Sturm et al.* [1998], showing that depth hoar fractions are highest during autumn, before decreasing during winter and spring.

[55] Similarities between both snow regimes were related to the seasonal progress of metamorphism and ablation. Generally, snow properties changed only moderately and snow survived the observation period in the ISPOL area. The formation of several ice layers within the snow was widespread and common for both snow regimes, but the overall metamorphism was weak compared to late summer snow covers [*Haas et al.*, 2001]. Even strong atmospheric signals, causing warm and moist air advection [*Willmes et al.*, 2006], did only affect near-surface snow properties with similar impact on all sites. Snow surface temperature was very similar on FYI and SYI, because with weak temperature gradients it is mainly determined by atmospheric conditions and less by of the underlying sea ice.

[56] For some snow properties, neither differences nor similarities could be quantified. This was mainly because of high uncertainties in the measuring techniques as well as strong lateral variability. Especially, snow density and wetness are difficult to measure, and single measurements are subject to high uncertainties. Additionally, high fractions of liquid water as well as the formation of ice layers make accurate measurements of snow properties difficult.

[57] Finally, it might be summarized that differences in snow properties are mainly caused by different underground (sea ice) conditions, while similarities are mainly related to surface heat fluxes, which are relatively similar over larger regions.

4.2. Snow Metamorphism and Moisture Transport

[58] Although our observations show some changes of snow properties in the transition from winter to summer, these changes were only subtle and the snow did not at all reach a highly metamorphic state as earlier observed for late January or February [*Haas et al.*, 2001]. This is because of the small atmospheric and oceanic heat fluxes, which are largely consumed by warming up the ice [*Haas et al.*, 2008a], because the heat capacity of sea ice increases exponentially at ice temperatures close to the melting point [*Yen et al.*, 1991]. Therefore, a state with totally isothermal snow was never reached during ISPOL, and only the upper snow layers were isotherm for a long while.

[59] In this state, energy is mainly consumed by the latent heat required for the internal melt, and the liquid water content can vary widely. As snow wetness measurements show (Figure 10), the snow cover was mostly in a pendular regime (liquid water content <8%), and meltwater was retained within the snow grain matrix [*Colbeck*, 1982]. Nevertheless, single measurements indicate that additional energy input occasionally increased snow wetness until parts of the snow cover entered the funicular regime and meltwater was able to percolate downward. This meltwater refroze in colder layers and contributed to formation of ice lenses and eventually superimposed ice. Rapid meltwater percolation, which could contribute to warming of the lower snow layers, as transport and refreezing of meltwater provide a source of sensible and latent heat, was not observed during ISPOL.

[60] On the contrary, the tracer experiments during the last week of ISPOL suggest a continued and quite intense downward meltwater flow, also into layers which were well below melting temperature. We are not sure how representative the tracer experiments really are, as the tracer might lead to preferential local melting at the molecular snow grain boundary layer. Additionally, SR is hydrophil, which may cause strong local anomalies on the microscale.

[61] However, meltwater could percolate along preferential pathways like percolation columns or ice pipes. It might be that these inhomogeneities can also lead to laterally highly inhomogeneous temperature fields, with confined regions of 0°C in the vicinity of these pipes. Meltwater pulses would temporarily warm the snow until the meltwater is refrozen. These features contribute to the generally large spatial variability and could have easily been missed by our temporally and spatially discontinuous measurements.

[62] *Vihma et al.* [2009] report a pronounced diurnal cycle of snow surface temperatures with an amplitude of 1.6°C for the entire observation period, whereas we state to have only small variability in snow surface temperatures after 1 December. This apparent discrepancy is mainly related to different methodology. Derived from long-wave radiation measurements (Figure 2), we find a similar diurnal cycle of surface temperatures, too. But this surface temperature represents only the topmost snow/water molecules (<1 mm), while handheld thermometer can only resolve the topmost millimeters to centimeters. Hence there exists a very strong temperature gradient in the topmost millimeter of the snow, which cannot be resolved by manual measurements. Beneath this, snow temperature varies only little as soon as it approaches its melting point temperature (0°C) because of increased snow wetness. Liquid water might act as an internal heat reservoir, and changes in heat fluxes result in microscale grain boundary freezing and melting, while the temperature remains constant. In contrast, during the first week of observations the entire snow cover was still colder and dryer, such that the diurnal cycle penetrated deeper into the snow cover and could be resolved by handheld thermometer measurements.

4.3. Superimposed Ice Formation

[63] During ISPOL, superimposed ice was formed only on FYI and was first found after 11 December. Extent and thickness were very heterogeneous on scales of decimeters. No gradual increase in amount, thickness, or consolidation could be observed. Parallel to our findings, *Tison et al.* [2008] observed the first formation of superimposed ice on the "clean site" of FY2 between 9 and 14 December. The approximately 5-cm-thick layer was found to impede gas exchange between sea ice and atmosphere. Furthermore, (fresh) snowmeltwater was hindered to enter the sea-ice brine network and affect biogeochemical processes.

[64] These findings of superimposed ice formation are consistent with our energy and mass balance studies. On the basis of potential snowmelt, as derived from the net heat flux into the snow, a superimposed ice thickness between 2 and 8 cm could have been expected. However, including the strong (36 to 51%) contribution of evaporation to the mass loss [*Nicolaus et al.*, 2006], the expected thickness of

superimposed ice reduces to 1 to 5 cm. From the presented snow mass loss of 27.3 (FY1) and 32.4 kg (SY1) a 3- to 4-cm-thick layer of superimposed ice could be formed. Hence, estimates from heat fluxes and mass balance match quite well.

[65] In contrast, the formation of superimposed ice was surprising with respect to the formation processes itself. On the basis of hitherto studies, superimposed ice formed always under melt conditions [*Granskog et al.*, 2006; *Jeffries et al.*, 1994; *Kawamura et al.*, 2004; *Koerner*, 1970; *Nicolaus et al.*, 2003], when temperature gradients were positive and the 0.0°C isotherm reached the snow-ice interface. However, these melt conditions were not fulfilled at any time of observation during ISPOL (Figure 7) [see also *Willmes et al.*, 2006], hence meltwater percolation is unlikely to be the major process of superimposed ice formation under these conditions. It is likely that the presented processes are typical for Antarctic sea-ice regions, where evaporation dominates snow ablation [*Nicolaus et al.*, 2006], while in all other regions, strong melt events dominate superimposed ice formation.

[66] On the basis of the above considerations about moisture transport within the snow cover, and the observed high spatial variability of snow properties, we assume that microscale variability of snow properties is most important for superimposed ice formation under low atmospheric energy input. The tracer studies and early results by *Colbeck* [1982] show that moisture can be transported comparably fast from the surface downward. Refreezing of this water due to colder snow, ice, or slush layers contributes to formation and growth of ice layers and ice lenses as well as superimposed ice. With increasing concentration and consolidation, ice layers and superimposed ice act as barriers for transport of water, water vapor, and gases through the snowpack. Well-consolidated layers of ice inhibit exchange of CO_2 between ocean/sea ice and atmosphere [*Tison et al.*, 2008]. Furthermore, it seems to be reasonable that superimposed ice has not formed under thicker second-year snow, because snowmelt was not strong enough for meltwater to penetrate through the thicker and colder snow cover on SYI to the snow-ice interface.

[67] In contrast to the findings on the ISPOL floe, a widespread formation of superimposed ice was found on the northern floes (EDGE and FIMR, Figure 1). This formation was probably related to stronger snowmelt, meltwater percolation, and refreezing on top of slush layers. Comparing these observations, a strong meridional gradient of snow and ice properties becomes obvious. This gradient is most likely caused by strong meteorological gradients in this region and their proximity to the ice edge. The ice edge region is more exposed to westerly winds, advecting warm air and moisture, including possible rain, while regions more to the south are dominated by cold easterly winds and cold air advection from the Antarctic ice sheet [*Willmes et al.*, 2009b]. Similar gradients can also be found in radar backscatter signatures [*Willmes et al.*, 2009b].

4.4. Role of Evaporation and Melt

[68] By means of theoretical considerations and in a modeling study, *Andreas and Ackley* [1982] and *Nicolaus et al.* [2006] have shown that the spring-to-summer evolution of snow and ice properties in the western Weddell Sea and in most other regions of the Southern Ocean are characterized by low atmospheric energy input, because of the dominance of turbulent fluxes and evaporation. As expected from those studies, about half of the net energy input was used up for warming of snow and sea ice, and less than 50% was used for snowmelt. No significant snowmelt was observed, and evaporation contributed over 40% to the observed snow mass loss. This means that all meltwater remained and refroze in the snowpack and the uppermost ice layers. Mass loss was most likely due to evaporation, while compaction and superimposed ice formation also contributed to snow thickness decrease. *Vihma et al.* [2009] find that approximately 0.15 cm d^{-1} (5 cm in 34 days) of snow thinning, not snow mass loss, were related to evaporation. This corresponds to 31% to 45% of the total snow thinning, as derived for different sites in this study (Table 1).

[69] Similarly to this, *Haas et al.* [2008a] have shown that hardly any sea-ice bottom melt occurred, either. Hence the observed freshening in the ocean surface layer [*Absy et al.*, 2008] is most likely a result of lateral sea ice and snowmelt as well as dissolution of snow and ice in leads.

5. Conclusions

[70] Even if snow on sea ice is extremely heterogeneous on all scales [*Massom et al.*, 2001; *Sturm et al.*, 1998] and several methodical difficulties occur during spring and summer snow observations, it is possible to distinguish snow regimes on FYI and SYI. General differences were found in snow thickness, basal and internal temperatures, and stratigraphy, because they are closely related to the underlying sea ice. In contrast, similarities were found in those physical properties, which are mainly controlled by atmospheric heat fluxes, like surface temperature, mass balance, and metamorphism.

[71] Snow metamorphism and ablation, as well as superimposed ice formation, progressed very slowly in the western Weddell Sea during late spring (December). The snow cover persisted into the summer on all sea-ice regimes of the ISPOL floe. This finding confirms studies by *Andreas and Ackley* [1982] and *Nicolaus et al.* [2006], who explain this persistence with strong turbulent heat fluxes, which cool the snow surface and reduce melting and are characteristic for snow on Antarctic sea ice. In any case, *Vihma et al.* [2009] point out that air masses can also cool significantly over sea ice and that cold and dry air masses are not always related to winds off the Antarctic continent. This discussion shows the need for developing improved methods for summer conditions with very small net fluxes.

[72] Corresponding to the findings of this study and those from physical sea-ice properties [*Haas et al.*, 2008a], *Schnack-Schiel et al.* [2008] found that stages of sea-ice inhabiting copepods represented also late winter-to-spring stages and that the main reproductive period had not begun until the end of ISPOL. Typical late spring and summer migration of copepods did not take place.

[73] Our observations show a strong meridional gradient (on a scale of 100 km) of snow properties and their related processes. This corresponds to earlier sea-ice studies in the Weddell Sea, showing how large scale atmospheric circulation affects snow and ice surface properties [*Simmonds and Keay*, 2000; *Venegas and Drinkwater*, 2001]. Addition-

ally, this implies the existence of similar gradients in biological processes and water mass composition, because both are highly sensitive to snow and sea-ice properties through its impact of fresh water entry and radiation transfer. In any case, it is difficult to draw general conclusions about strength and extent of meridional gradients, because they also depend on prevailing wind direction and properties of advected air masses, as they could either be comparably warm and moist when coming from open ocean areas or cold and dry air when originating from inland ice masses or traveling long over sea ice [*Vihma et al.*, 2009].

[74] Our results may also be used for the validation or initialization of numerical simulations. We expect studies focusing on the annual cycle of snow on sea ice to benefit most [e.g., *Cheng et al.*, 2008; *Vancoppenolle et al.*, 2009], but also large-scale simulations might benefit from the described properties and processes, as snow processes are of critical importance for interaction between sea ice and atmosphere (including forcing data sets). Our data also provide important ground truth for remote sensing projects, strongly depending on physical snow properties [*Barber et al.*, 1998; *Haas et al.*, 2001, 2008a; *Willmes et al.*, 2006, 2009a]. Airborne measurements of ice thickness depend on reliable data of snow thickness and/or density [*Haas et al.*, 2008b]. Therefore our detailed measurements of snow thickness and physical surface properties are expected to be most valuable.

[75] Finally, the drift with the ISPOL floe was too short to observe the main changes during spring-summer transition. Snow metamorphism and sea-ice changes were not yet strong enough to trigger significant changes and to initiate typical summer sea-ice processes. Therefore, upcoming drift experiments should continue longer into the summer season or include regular observations in the marginal ice zone, in order to increase the understanding of main changes during spring. In order to extend this study in space and time, observations from autonomous measuring buoys, e.g., drifting ice mass balance buoys [e.g., *Perovich et al.*, 2008], could be included for upcoming studies.

[76] **Acknowledgments.** We are most grateful to Anja Nicolaus (Alfred Wegener Institute for Polar and Marine Research) for her assistance with field measurements and sample processing. We thank Jouko Launiainen, Milla Johansson, and Pekka Kosloff (all Finnish Institute for Marine Research) for sharing their meteorological observations and energy balance measurements with us, as well as for profitable discussion of the results during the preparation of this manuscript. The assistance of the captain and the crew of the ISPOL cruise and the great cooperation with the scientific ship party are highly appreciated. Timo Vihma (Finnish Meteorological Institute) and one anonymous reviewer contributed with constructive comments to improving the manuscript. This study was funded by the Alfred Wegener Institute for Polar and Marine Research.

References

Absy, J. M., M. Schröder, R. Muench, and H. H. Hellmer (2008), Early summer thermohaline characteristics and mixing in the western Weddell Sea, *Deep Sea Res., Part II*, *55*, 1117–1131, doi:10.1016/j.dsr2.2007.12.023.

Allison, I., R. E. Brandt, and S. G. Warren (1993), East Antarctic sea ice: Albedo, thickness distribution, and snow cover, *J. Geophys. Res.*, *98*(C7), 12,417–12,429, doi:10.1029/93JC00648.

Anderson, M. R., and S. D. Drobot (2001), Spatial and temporal variability in snowmelt onset over Arctic sea ice, *Ann. Glaciol.*, *33*, 74–78, doi:10.3189/172756401781818284.

Andreas, E. L., and S. F. Ackley (1982), On the differences in ablation seasons of Arctic and Antarctic sea ice, *J. Atmos. Sci.*, *39*(2), 440–447, doi:10.1175/1520-0469(1982)039<0440:OTDIAS>2.0.CO;2.

Barber, D. G., A. Thomas, and T. N. Papakyriakou (1998), Role of SAR in surface energy flux measurements over sea ice, in *Analysis of SAR Data of the Polar Oceans: Recent Advances*, edited by C. Tsatsoulis and R. Kwok, pp. 35–67, Springer, Berlin.

Bareiss, J., and K. Görgen (2008), ISPOL weather conditions in the context of long-term climate variability in the north-western Weddell Sea, *Deep Sea Res., Part II*, *55*, 918–932, doi:10.1016/j.dsr2.2007.12.017.

Bock, K. H., K. Bult, and R. Hartig (2007), General weather conditions during ANT XXII/2, in *The Expeditions ANTARKTIS XXII/1 and XXII/2 of the Research Vessel "Polarstern" in 2004/2005*, edited by S. El Naggar et al., pp. 47–52, Alfred Wegener Inst. for Polar and Mar. Res., Bremerhaven, Germany.

Cheng, B., Z. Zhang, T. Vihma, M. M. Johansson, L. Bian, Z. Li, and H. Wu (2008), Model experiments on snow and ice thermodynamics in the Arctic Ocean with CHINARE 2003 data, *J. Geophys. Res.*, *113*, C09020, doi:10.1029/2007JC004654.

Colbeck, S. C. (1982), The geometry and permittivity of snow at high frequencies, *J. Appl. Phys.*, *53*(6), 4495–4500, doi:10.1063/1.331186.

Colbeck, S. C., E. Akitaya, R. Armstrong, H. Grubler, J. Lafeuille, K. Lied, D. McClung, and E. Morris (1990), *The International Classification for Seasonal Snow on the Ground*, Cold Reg. Res. and Eng. Lab., Hanover, N. H.

Curry, J. A., J. L. Schramm, D. K. Perovich, and J. O. Pinto (2001), Applications of SHEBA/FIRE data to evaluation of snow/ice albedo parameterizations, *J. Geophys. Res.*, *106*(D14), 15,345–15,355, doi:10.1029/2000JD900311.

Eicken, H., M. A. Lange, H. W. Hubberten, and P. Wadhams (1994), Characteristics and distribution patterns of snow and meteoric ice in the Weddell Sea and their contribution to the mass balance of sea ice, *Ann. Geophys.*, *12*, 80–93, doi:10.1007/s00585-994-0080-x.

Eicken, H., H. Fischer, and P. Lemke (1995), Effects of the snow cover on Antarctic sea ice and potential modulation of its response to climate change, *Ann. Glaciol.*, *21*, 369–376.

Freitag, J., and H. Eicken (2003), Meltwater circulation and permeability of Arctic summer sea ice derived from hydrological field experiments, *J. Glaciol.*, *49*(166), 349–358, doi:10.3189/172756503781830601.

Frolov, I. E., Z. M. Gudkovich, V. F. Radionov, A. V. Shirochkov, and L. A. Timokhov (2005), *The Arctic Basin: Results from the Russian Drifting Stations*, Springer, Berlin.

Gascard, J.-C., et al. (2008), Exploring Arctic transpolar drift during dramatic sea ice retreat, *EOS Trans. AGU*, *89*(3), 21–28, doi:10.1029/2008EO030001.

Granskog, M. A., T. Vihma, R. Pirazzini, and B. Cheng (2006), Superimposed ice formation and surface energy fluxes on sea ice during the spring melt-freeze period in the Baltic Sea, *J. Glaciol.*, *52*(176), 119–127, doi:10.3189/172756506781828971.

Grenfell, T. C., and D. K. Perovich (1984), Spectral albedos of sea ice and incident solar irradiance in the southern Beaufort Sea, *J. Geophys. Res.*, *89*(C3), 3573–3580, doi:10.1029/JC089iC03p03573.

Haas, C., D. N. Thomas, and J. Bareiss (2001), Surface properties and processes of perennial Antarctic sea ice in summer, *J. Glaciol.*, *47*, 613–625, doi:10.3189/172756501781831864.

Haas, C., M. Nicolaus, S. Willmes, A. Worby, and D. Flinspach (2008a), Sea ice and snow thickness and physical properties of an ice floe in the western Weddell Sea and their changes during spring warming, *Deep Sea Res., Part II*, *55*, 963–974, doi:10.1016/j.dsr2.2007.12.020.

Haas, C., A. Pfaffling, S. Hendricks, L. Rabenstein, J.-L. Etienne, and I. Rigor (2008b), Reduced ice thickness in Arctic Transpolar Drift favors rapid ice retreat, *Geophys. Res. Lett.*, *35*, L17501, doi:10.1029/2008GL034457.

Heil, P., J. K. Hutchings, A. P. Worby, M. Johansson, J. Launiainen, C. Haas, and W. D. Hibler III (2008), Tidal forcing on sea-ice drift and deformation in the western Weddell Sea in early austral summer, 2004, *Deep Sea Res., Part II*, *55*, 943–962, doi:10.1016/j.dsr2.2007.12.026.

Hellmer, H. H., M. Schröder, C. Haas, G. S. Dieckmann, and M. Spindler (2008), The ISPOL drift experiment, *Deep Sea Res., Part II*, *55*, 913–917, doi:10.1016/j.dsr2.2008.01.001.

Holland, M. M., C. M. Bitz, A. J. Weaver, and M. Eby (2001), The influence of sea ice physics on simulations of climate change, *J. Geophys. Res.*, *106*(C9), 19,639–19,655, doi:10.1029/2000JC000651.

Jeffries, M. O., R. A. Shaw, K. Morris, A. L. Veazey, and H. R. Krouse (1994), Crystal structure, stable isotopes δ^{18}O and development of sea ice in the Ross, Amundsen and Bellinghausen Seas, Antarctica, *J. Geophys. Res.*, *99*(C1), 985–995, doi:10.1029/93JC02057.

Jeffries, M. O., A. P. Worby, K. Morris, and W. F. Weeks (1997), Seasonal variations in the properties and structural composition of sea ice and snow cover in the Bellinghausen and Amundsen Sea, Antarctica, *J. Glaciol.*, *43*(143), 138–151.

Jordan, R. E. (1991), A one-dimensional temperature model for a snow cover, *Spec. Rep. 91-16*, U.S. Army Corps of Eng. Cold Reg. Res. and Eng. Lab., Hanover, N. H.

Kawamura, T., K. I. Ohshima, T. Takizawa, and S. Ushio (1997), Physical, structural and isotopic characteristics and growth processes of fast sea ice in Lützow-Holm Bay, Antarctica, *J. Geophys. Res.*, *102*(C2), 3345–3355, doi:10.1029/96JC03206.

Kawamura, T., M. O. Jeffries, J. L. Tison, and H. R. Krouse (2004), Superimposed ice formation in summer on Ross Sea pack ice floes, *Ann. Glaciol.*, *39*, 563–568, doi:10.3189/172756404781814168.

Koerner, R. M. (1970), Some observations on superimposition on ice on the Devon Island Ice Cap, N.W.T. Canada, *Geogr. Ann., Ser. A*, *52*, 57–67.

Launiainen, J., and B. Cheng (1995), A simple non-iterative algorithm for calculating turbulent bulk fluxes in diabatic conditions over water snow/ice and ground surface, *Rep. Ser. Geophys.*, vol. 33, 15 pp., Dept. of Geophys., Univ. of Helsinki, Helsinki.

Massom, R. A., M. R. Drinkwater, and C. Haas (1997), Winter snow cover on sea ice in the Weddell Sea, *J. Geophys. Res.*, *102*(C1), 1101–1117, doi:10.1029/96JC02992.

Massom, R. A., V. I. Lytle, A. P. Worby, and I. Allison (1998), Winter snow cover variability on East Antarctic sea ice, *J. Geophys. Res.*, *103*(C11), 24,837–24,855, doi:10.1029/98JC01617.

Massom, R. A., et al. (2001), Snow on Antarctic sea ice, *Rev. Geophys.*, *39*(3), 413–445, doi:10.1029/2000RG000085.

Maykut, G. A. (1986), The surface heat and mass balance, in *Geophysics of Sea Ice*, edited by N. Untersteiner, pp. 395–463, NATO ASI Ser., New York.

Maykut, G. A., and N. Untersteiner (1971), Some results from a time-dependent thermodynamic model of sea ice, *J. Geophys. Res.*, *76*(6), 1550–1575, doi:10.1029/JC076i006p01550.

McPhee, M. G. (2008), Physics of early summer ice/ocean exchanges in the western Weddell Sea during ISPOL, *Deep Sea Res., Part II*, *55*, 1075–1097, doi:10.1016/j.dsr2.2007.12.022.

Morris, K., and M. O. Jeffries (2001), Seasonal contrasts in snow-cover characteristics on Ross Sea ice floes, *Ann. Glaciol.*, *33*, 61–68, doi:10.3189/172756401781818608.

Nicolaus, M., C. Hass, and J. Bareiss (2003), Observations of superimposed ice formation at melt-onset on fast ice on Kongsfjorden, Svalbard, *Phys. Chem. Earth*, *28*, 1241–1248.

Nicolaus, M., C. Haas, J. Bareiss, and S. Willmes (2006), A model study of differences of snow thinning on Arctic and Antarctic first-year sea ice during spring and summer, *Ann. Glaciol.*, *44*, 147–153, doi:10.3189/172756406781811312.

Ohshima, K. I., K. Yoshida, H. Shimoda, M. Wakatsuchi, T. Endoh, and M. Fukuchi (1998), Relationship between the upper ocean and sea ice during the Antarctic melting season, *J. Geophys. Res.*, *103*(C4), 7601–7615, doi:10.1029/97JC02806.

Perovich, D. K. (1996), *The Optical Properties of Sea Ice*, Cold Reg. Res. and Eng. Lab., Hanover, N. H.

Perovich, D. K. (2005), On the aggregate-scale partitioning of solar radiation in Arctic sea ice during the Surface Heat Budget of the Arctic Ocean (SHEBA) field experiment, *J. Geophys. Res.*, *110*, C03002, doi:10.1029/2004JC002512.

Perovich, D. K., et al. (1999), Year on ice gives climate insights, *Eos Trans. AGU*, *80*(41), 485–486.

Perovich, D. K., T. C. Grenfell, B. Light, and P. V. Hobbs (2002), Seasonal evolution of the albedo of multiyear Arctic sea ice, *J. Geophys. Res.*, *107*(C10), 8044, doi:10.1029/2000JC000438.

Perovich, D. K., J. A. Richter-Menge, K. F. Jones, and B. Light (2008), Sunlight, water, and ice: Extreme Arctic sea ice melt during the summer of 2007, *Geophys. Res. Lett.*, *35*, L11501, doi:10.1029/2008GL034007.

Schnack-Schiel, S. B., C. Haas, J. Michels, E. Mizdalski, H. Schünemann, M. Steffens, and D. N. Thomas (2008), Copepods in sea ice of the western Weddell Sea during austral spring 2004, *Deep Sea Res., Part II*, *55*, 1056–1067, doi:10.1016/j.dsr2.2007.12.014.

Sihvola, A., and M. Tiuri (1986), Snow fork for field determination of the density and wetness profiles of a snow pack, *IEEE Trans. Geosci. Remote Sens.*, *GE-24*(5), 717–721, doi:10.1109/TGRS.1986.289619.

Simmonds, I., and K. Keay (2000), Mean southern hemisphere extratropical cyclone behaviour in the 40-year NCEP-NCAR reanalysis, *J. Clim.*, *13*, 873–885, doi:10.1175/1520-0442(2000)013<0873:MSHECB>2.0.CO;2.

Sturm, M., K. Morris, and R. Massom (1998), The winter snow cover of the West Antarctic pack ice: Its spatial and temporal variability, in *Antarctic Sea Ice: Physical Processes, Interactions and Variability*, edited by M. O. Jeffries, pp. 1–18, AGU, Washington, D. C.

Tison, J. L., A. Worby, B. Delille, F. Brabant, S. Papadimitriou, D. Thomas, J. de Jong, D. Lannuzel, and C. Haas (2008), Temporal evolution of decaying summer first-year sea ice in the western Weddell Sea, Antarctica, *Deep Sea Res., Part II*, *55*, 975–987, doi:10.1016/j.dsr2.2007.12.021.

Tonboe, R., S. Andersen, and L. T. Pedersen (2006), Simulation of the Ku-band radar altimeter sea ice effective scattering surface, *IEEE Geosci. Remote Sens. Lett.*, *3*(2), 237–240, doi:10.1109/LGRS.2005.862276.

Vancoppenolle, M., T. Fichefet, and H. Goosse (2009), Simulating the mass balance and salinity of Arctic and Antarctic sea ice: 2. Importance of sea ice salinity variations, *Ocean Modell.*, *27*, 54–69, doi:10.1016/j.ocemod.2008.11.003.

Venegas, S. A., and M. R. Drinkwater (2001), Sea ice, atmosphere and upper ocean variability in the Weddell Sea, Antarctica, *J. Geophys. Res.*, *106*(C8), 16,747–16,765, doi:10.1029/2000JC000594.

Vihma, T., J. Launiainen, and J. Uotila (1996), Weddell Sea ice drift: Kinematics and wind forcing, *J. Geophys. Res.*, *101*(C8), 18,279–18,296, doi:10.1029/96JC01441.

Vihma, T., M. M. Johansson, and J. Launiainen (2009), Radiative and turbulent surface heat fluxes over sea ice in the western Weddell Sea in early summer, *J. Geophys. Res.*, *114*, C04019, doi:10.1029/2008JC004995.

Warren, S. G., I. G. Rigor, N. Untersteiner, V. F. Radionov, N. N. Bryazgin, Y. I. Aleksandrov, and R. Colony (1999), Snow depth on Arctic sea ice, *J. Clim.*, *12*(6), 1814–1829, doi:10.1175/1520-0442 (1999)012<1814:SDOASI>2.0.CO;2.

Willmes, S., J. Bareiss, C. Haas, and M. Nicolaus (2006), The importance of diurnal processes for the seasonal cycle of sea-ice microwave brightness temperatures during early summer in the Weddell Sea, Antarctica, *Ann. Glaciol.*, *44*, 297–302, doi:10.3189/172756406781811817.

Willmes, S., C. Haas, J. Bareiss, and M. Nicolaus (2009a), Satellite microwave observations of the interannual variability of snowmelt on sea ice in the Southern Ocean, *J. Geophys. Res.*, *114*, C03006, doi:10.1029/2008JC004919.

Willmes, S., C. Haas, M. Nicolaus, and J. Bareiss (2009b), High radar-backscatter regions on Antarctic sea ice and their relation to sea-ice and snow properties and meteorological conditions, *Int. J. Remote Sens.*, in press.

Winebrenner, D. P., D. G. Long, and B. Holt (1998), Mapping the progression of melt onset and freeze-up on Arctic sea ice using SAR and scatterometry, in *Analysis of SAR Data of the Polar Oceans: Recent Advances*, edited by C. Tsatsoulis and R. Kwok, pp. 129–144, Springer, Berlin.

Yen, Y. C., K. C. Chen, and S. Fukusako (1991), Review of intrinsic thermophysical properties of snow, ice, sea ice, and frost, in *Proceedings 3rd International Symposium on Cold Regions Heat Transfer*, edited by J. P. Zarling and S. L. Faussett, pp. 187–218, Univ. of Alaska, Fairbanks.

C. Haas, Earth and Atmospheric Sciences, University of Alberta, 1-26 Earth Sciences Building, Edmonton, AB T6G 2E3, Canada. (christian.haas@ualberta.ca)

M. Nicolaus, Norwegian Polar Institute, Polar Environmental Centre, N-9296 Tromsø, Norway. (marcel.nicolaus@npolar.no)

S. Willmes, Environmental Meteorology, University of Trier, Trier D-54286, Germany. (willmes@un-trier.de)